









Geophysical Research Letters[®]



RESEARCH LETTER

10.1029/2021GL095413

Structure and Stress Field of the Lithosphere Between Pamir and Tarim

Wasja Bloch^{1,2} , Bernd Schurr¹ , Xiaohui Yuan¹ , Lothar Ratschbacher³ , Sanaa Reuter³ , Sofia-Katerina Kufner^{1,4} , Qiang Xu^{5,6} , and Junmeng Zhao^{5,6} 

¹GFZ German Research Centre for Geosciences, Potsdam, Germany, ²Now at Earth, Ocean and Atmospheric Sciences, University of British Columbia, Vancouver, BC, Canada, ³Geologie, Technische Universität Bergakademie Freiberg, Freiberg, Germany, ⁴British Antarctic Survey, Cambridge, England, ⁵Key Laboratory of Continental Collision and Plateau Uplift, Institute of Tibetan Plateau Research, Chinese Academy of Sciences, Beijing, China, ⁶CAS Center for Excellence in Tibetan Plateau Earth Sciences, Beijing, China

Key Points:

- New local earthquake catalog and seismic *P*-wave velocity model for the eastern Pamir
- Elevated velocities outline the northern and eastern margin of the Indian mantle indenter beneath the Pamir plateau
- The indenter overturns the eastern end of the Asian slab and terminates along a transform margin against the Tarim block

Supporting Information:

Supporting Information may be found in the online version of this article.

Correspondence to:

W. Bloch,
wbloch@eoas.ubc.ca

Citation:

Bloch, W., Schurr, B., Yuan, X., Ratschbacher, L., Reuter, S., Kufner, S.-K., et al. (2021). Structure and stress field of the lithosphere between Pamir and Tarim. *Geophysical Research Letters*, 48, e2021GL095413. <https://doi.org/10.1029/2021GL095413>

Received 30 JUL 2021

Accepted 5 OCT 2021

Abstract The Pamir plateau protrudes ~300 km between the Tajik- and Tarim-basin lithosphere of Central Asia. Whether its salient location and shape are caused by forceful indentation of a promontory of Indian mantle lithosphere is debated. We present a new local-seismicity and focal-mechanism catalog, and a *P*-wave velocity model of the eastern part of the collision system. The data suggest a south-dipping Asian slab that overturns in its easternmost segment. The largest principal stress at depth acts normal on the slab and is orientated parallel to the plate convergence direction. In front (south) of the Asian slab, a volume of mantle with elevated velocities and lined by weak seismicity constitutes the postulated Indian mantle indenter. We propose that the indenter delaminates and overturns the Asian slab, underthrusts the Tarim lithosphere along a compressive transform boundary, and controls the location and shape of the Pamir plateau.

Plain Language Summary The Pamir plateau stands out between the Tajik basin to the west and the Tarim basin to the east. Its location and shape are either caused by a part of the Indian continent that protrudes below Pamir's crust, or thinned lithosphere of a former Asian basin existed in the place of the Pamir and subducted during the collision of India with Asia. Our new seismological data show that the Asian slab—a displaced part or slice of the Tarim-Tajik-basin lithosphere—is overturned beneath the eastern Pamir. A zone of high seismic velocities, indicative of a relatively cold and rigid mantle lithosphere, occurs in front (south) of the Asian slab. A seismically active zone with low seismic velocities is squeezed between this structure and the Tarim lithosphere. Together, these observations trace the northern and eastern margin of the Indian mantle indenter that predefines the shape of the Pamir plateau.

1. Introduction

The salient Pamir plateau is part of the India-Asia collision system. It is offset by ~300 km to the north in relation to the adjacent Tibet plateau and protrudes between the Tajik basin in the west and the cratonic block of the Tarim basin in the east (e.g., Lu et al., 2008). The northern Pamir and the Kunlun of northwestern Tibet comprise subduction-accretion-arc complexes accreted to and built on Asian continental basement. The central and southern Pamir and the Karakorum and Hindu-Kush represent Gondwana-derived microcontinents and subduction-accretion-arc complexes (Figure 1; Burtman & Molnar, 1993; Schwab et al., 2004).

Beneath the Pamir, a band of intermediate-depth (50–250 km) earthquakes, extending from the southwestern Pamir northeastward into the central Pamir, bends eastward, and shows diminished earthquake activity beneath the eastern Pamir (Figure 2; Pegler & Das, 1998; Sipp, Schurr, Yuan, et al., 2013). Receiver function images (Schneider et al., 2013) and the analysis of guided waves (Mechie et al., 2019) show that the earthquakes in the western and central Pamir reside in a 10–15 km thick, E- to S-dipping low velocity zone (LVZ) connected to the Asian lithosphere; seismic velocities indicate that the LVZ represents continental crust, which has—together with the underlying mantle lithosphere—been interpreted as the Asian slab (Mechie et al., 2019; Schneider et al., 2013; Sippl, Schurr, Tympel, et al., 2013). Beneath the northwestern Kunlun,

© 2021. The Authors.

This is an open access article under the terms of the [Creative Commons Attribution License](https://creativecommons.org/licenses/by/4.0/), which permits use, distribution and reproduction in any medium, provided the original work is properly cited.

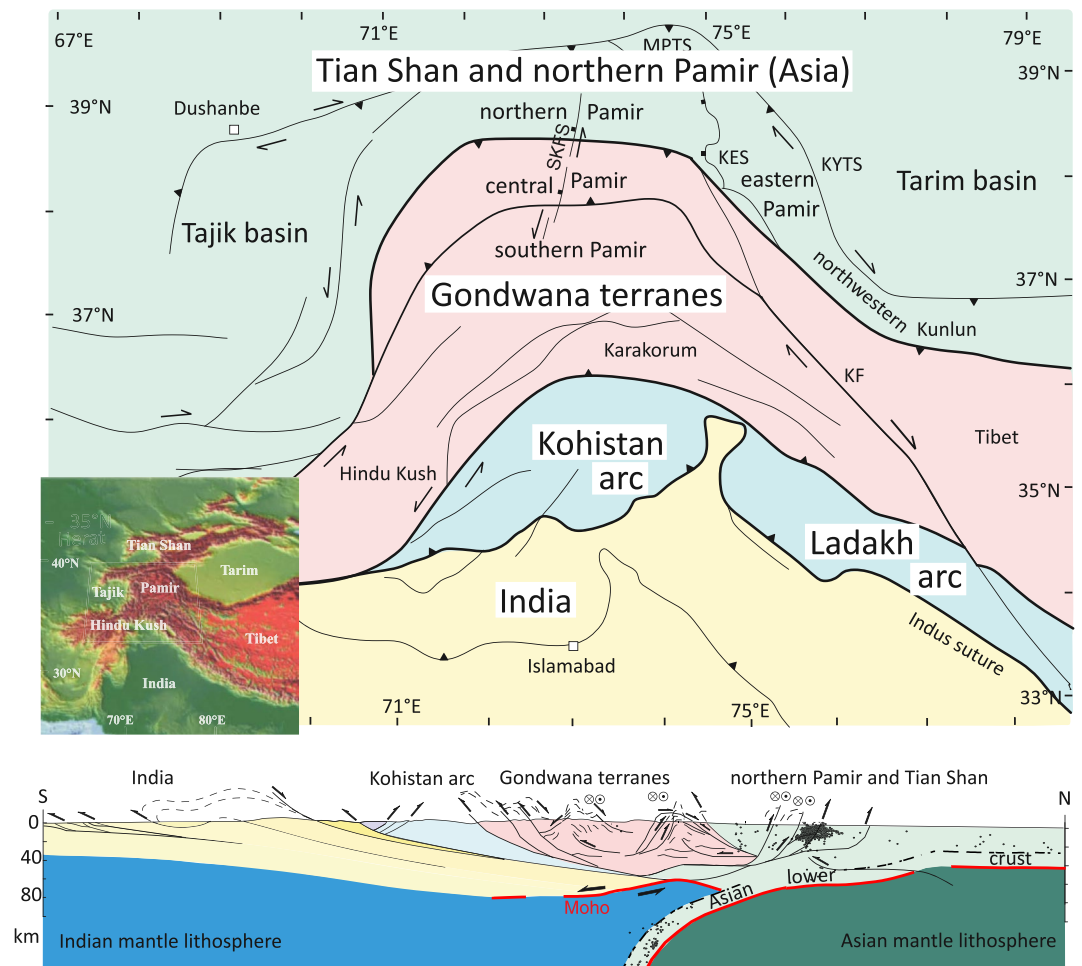


Figure 1. Tectonic units of the Pamir in map view and as a schematic cross section along $\sim 74^\circ\text{E}$. Deep structure mostly from (Schneider et al., 2013). KES: Kongur Extensional System; KF: Karakorum Fault; KYTS: Kashgar-Yecheng Transfer System; MPTS: Main Pamir Thrust System; SKFS: Sarez-Karakul Fault System.

diffuse seismicity at 100–150 km depth was attributed to Tarim lithosphere underthrusting the Pamir (Fan et al., 1994; Pegler & Das, 1998).

To understand the oroclinal shape of the Pamir, the intermediate-depth seismicity beneath the Hindu-Kush, Pamir and Kunlun, and the along-strike changes of the deep structure from the Hindu-Kush through the Pamir to Tibet and the Himalaya, it is a key to know whether Asian lithosphere subducts as a narrow, back-rolling slab of thinned crust (Burtman & Molnar, 1993; Sobel et al., 2013) or if Asian lower crust and mantle lithosphere is forced to subduct/delaminate due to indentation by cratonic Indian mantle lithosphere (Kufner et al., 2016; Metzger et al., 2017). If an indenter governs the shape of the Pamir plateau, its properties can best be characterized at its margins, where it interacts with and has a detectable contrast to the bounding units. For the western margin, Kufner, Schurr, et al. (2018) argued that a sinistral-oblique transform margin separates indenting cratonic Indian mantle lithosphere beneath the Pamir from subducting Indian continental-margin lithosphere below the Hindu-Kush. The subduction model postulates rollback of a narrow Asian slab of thinned continental crust that involves mantle corner flow and a subduction-transform edge propagator fault, separating the subducting Asian slab and its hanging wall from the Tarim block to the east. Geophysical data indicate that the hinterland crust is not thinned (>50 km; Schneider et al., 2019), questioning the premise of the rollback model, because thick buoyant continental crust typically does not subduct beneath a continent as a whole (e.g., Kelly & Beaumont, 2021; Z.-H. Li et al., 2016). The indentation model involves forced Asian slab subduction and delamination due to flat-slab underthrusting of a mechanically strong Indian continental lithospheric mantle indenter, a process recently

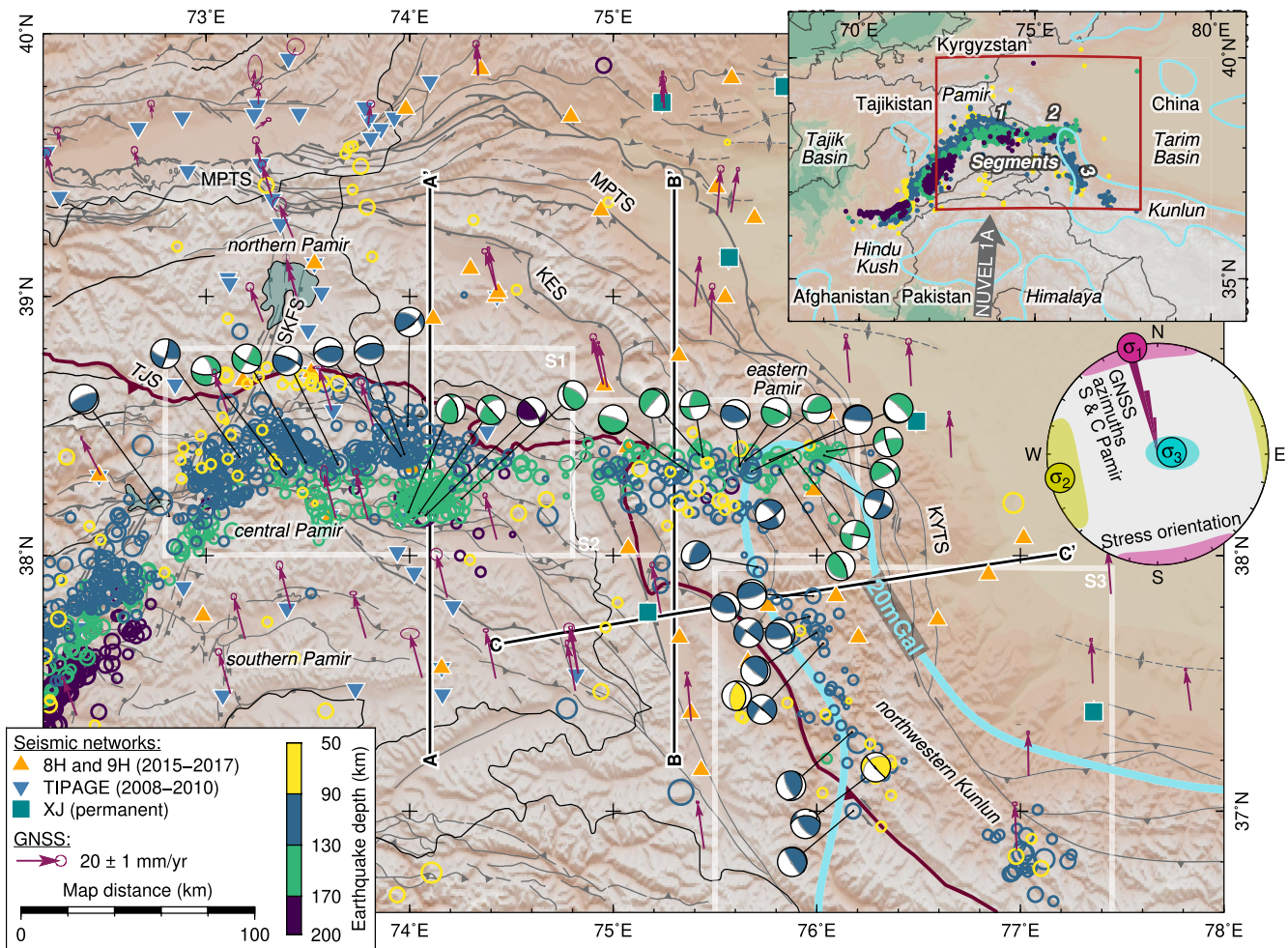


Figure 2. Seismotectonic map of the Pamir and northwestern Kunlun with seismic networks, seismicity at intermediate depth, focal mechanisms (black and gray nodal planes indicate fault and auxiliary plane preferred by stress inversion), global navigation satellite system (GNSS) velocity field (Ischuk et al., 2013; Zubovich et al., 2010), and 20 mGal positive isostatic gravity anomaly (Balmino et al., 2012). Abbreviations as in Figure 1. TJS: Tanyamas-Jinsha suture; S1, S2, S3: segments 1 to 3; Map inset: Regional overview. Stereo-net inset: Lower hemisphere stereographic projection of stress directions and 95% confidence ellipsoids (Figure S16 in Supporting Information S1) and histogram of GNSS azimuths in the southern and central Pamir (<38.8°N, 73–77°E, 5° bins).

modeled for the Pamir (Kelly & Beaumont, 2021). The indenter is imaged by refraction seismology and local body wave tomography as a high velocity zone (HVZ) south of the Asian slab (Mechie et al., 2012; Sippl, Schurr, Tymphel, et al., 2013). Teleseismic body and surface wave tomography shows that it connects with the exposed Indian craton (e.g., Agius & Lebedev, 2013; C. Li et al., 2008; Liang et al., 2020; van Hinsbergen et al., 2019); its northern extent remained unresolved due to the smearing of the indenter HVZ with the HVZ that represents cratonic Asia.

Herein, intermediate-depth earthquakes, focal-mechanism based stress data, and a P -wave velocity (V_p) model derived from new and published local seismological data in companionship with new receiver functions (Xu et al., 2021) illuminate the lithospheric configuration of the central and eastern Pamir and the boundary zone with the Tarim craton. Our data characterize the northern tip of an indenter—interpreted as a promontory of Indian mantle lithosphere—and its eastern edge, where it underthrusts on the lithosphere of the Tarim block.

2. Data and Methods

We used seismograms recorded with two new local seismic networks that were in operation between August 2015 and July 2017 in the eastern Pamir, northwestern Kunlun, and northwestern Tarim basin (Text S1 in Supporting Information S1; Yuan, Schurr, Bloch, et al., 2018; Yuan, Schurr, Kufner, & Bloch, 2018) and additional regional stations (PMP International (Tajikistan), 2005; SEISDMC, 2021). We detected seismic events using a waveform-envelope-coherence-based approach (Comino et al., 2017) and picked *P*- and *S*-wave arrival times using calibrated automatic picking algorithms (Text S2 in Supporting Information S1; Aldersons, 2004; Diehl et al., 2009).

Using additional data of an existing earthquake catalog from the western and central Pamir (Sippl, Schurr, Tympel, et al., 2013), we inverted for the 3-D subsurface V_p structure (Thurber, 1983). We masked out poorly resolved volumes of the tomogram based on a checkerboard resolution test and performed synthetic recovery tests for the anomalies that are most important to our interpretation (Text S3 and Figures S1–S11 in Supporting Information S1).

We jointly located the newly and previously (Sippl, Schurr, Tympel, et al., 2013) detected seismicity at intermediate depth in the 3-D V_p model, assessed location uncertainties (Lomax et al., 2000) and performed a relative event relocation for events that were <10 km apart (Waldhauser & Ellsworth, 2000) (Text S4 and Figures S12–S15 in Supporting Information S1), yielding a unified catalog of 1,493 events at intermediate depth.

We determined focal mechanisms of the strongest of the newly located events and inverted for the deviatoric unit stress tensor from which we report the orientation of the three principal axes ($\sigma_1 > \sigma_2 > \sigma_3$), orientation uncertainties, and relative stress magnitudes (Text S5 and Figure S16 in Supporting Information S1). The seismicity catalog (Data Set S1), focal mechanism catalog (Data Set S2), and the V_p structure (Data Set S3) are published in the Supporting Information S1 and Bloch, Schurr et al. (2021).

3. Seismicity

Crustal seismicity of the upper 30 km is dominated by the aftershock sequences of strong earthquakes that struck the Pamir in 2015/16 (Bloch, Metzger, et al., 2021) and is omitted from the main figures. The middle and lower crust (30–50 km depth) is essentially aseismic (Figure S2 in Supporting Information S1). Intermediate-depth earthquakes in the central and eastern Pamir could be localized with a median (5%–95% quantile) uncertainty of 2.3 (1.1–6.4) km in longitudinal direction, 2.0 (1.0–5.0) km in latitude and 3.2 (1.8–9.4) km in depth (Figure S15 in Supporting Information S1). They outline three steeply dipping, planar to curvilinear segments separated by regions of sparse seismicity (Figures 2 and 3).

Segment 1 begins at 72.8°E, 38°N, in continuation of the NE-striking, planar, seismically active structure farther to the southwest (Figure 2; Schneider et al., 2013; Sippl, Schurr, Yuan, et al., 2013). It forms an S- to SE-dipping band between 73.0°E and 74.3°E, and shows vigorous seismicity between 70–180 km depth in its easternmost part (Figures 3a and S12 in Supporting Information S1); farther east, seismic activity decreases.

Segment 2 in the eastern Pamir—in the direct continuation of segment 1—contains a few earthquakes at 50–80 km depth in a S-dipping structure. Below, at 80–170 km depth, the earthquake-defined band dips N (Figure 2, dotted lines in Figures 3b and S14g–S14i in Supporting Information S1). Seismicity in segment 2 is less intense compared to segment 1 (Figure S12 in Supporting Information S1).

Seismicity in segment 3 forms a continuous, NNW-striking structure at 80–120 km depth between 37°N and 38°N; it follows the northwestern Kunlun (Figures 2 and 3c). Seismic activity is comparably weak (Figure S12 in Supporting Information S1).

In all segments, focal mechanisms show dominantly thrust and subordinately strike-slip faulting. Accordingly, the regional stress tensor at intermediate depth indicates a thrust regime with a near-horizontal σ_1 , trending N13°W \pm 60° (95% confidence interval) and near vertical σ_3 (Figure 2). Inverting for the stress of the three segments separately yields similar directions, despite strongly variable uncertainties due to the disparate amounts of data (Figure S16 in Supporting Information S1). The azimuth of σ_1 is about parallel to

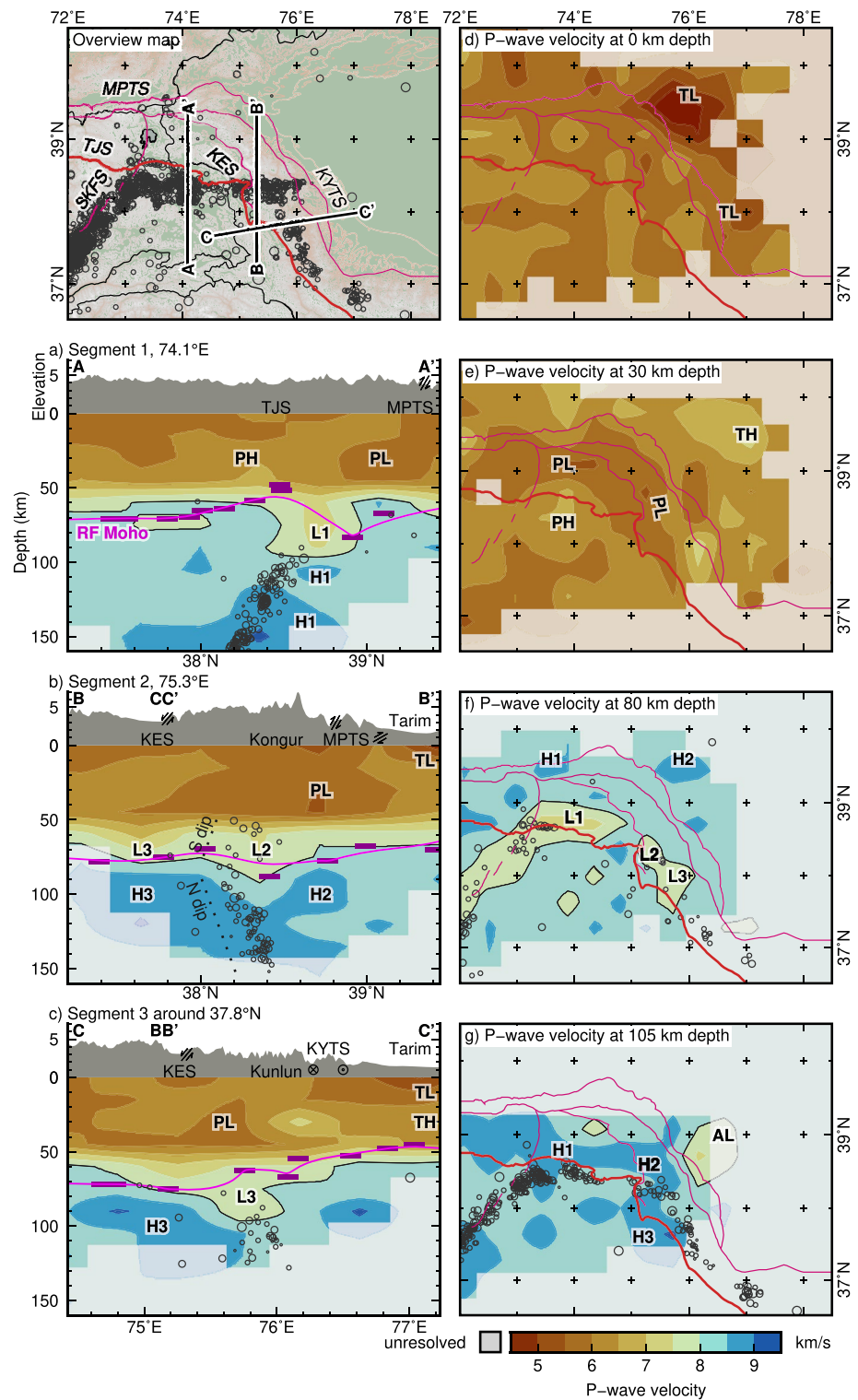


Figure 3. Sections through the tomogram. (a–c) Profiles shown on overview map; swath width ± 25 km; no vertical exaggeration in the depth profiles. Dark/light magenta: Receiver function Moho at individual stations and interpolated depth (Schneider et al., 2019; Xu et al., 2021). (d–g) Horizontal sections. TH, PH, H1, H2, H3: high V_p zones. TL, PL, L1, L2, L3, AL: low V_p zones. Poorly resolved areas were masked based on a resolution test (Text S3 in Supporting Information S1). Relative V_p anomalies with respect to the background model are shown in Figure S11 in Supporting Information S1.

the azimuth of the GNSS vectors in the southern and central Pamir (south of 38.8°N), N12°W ±4° (Figure 2; Ischuk et al., 2013; Zubovich et al., 2010).

4. Velocity Structure

In the shallow crust, the sedimentary rock section of the Tarim basin is characterized by $V_p < 5$ km/s (*TL* in Figures 3b–3d). In the middle-lower crust, the Tarim basement appears discontinuously with $V_p = 6.5$ –7.5 km/s (*TH* in Figures 3c and 3e) close to the poor-resolution rim of the tomographic volume. A LVZ is located in the mantle of northwestern Tarim (*AL* in Figure 3g). An arcuate crustal LVZ with $V_p = 5$ –6 km/s—lower than the overburden and the background velocity at this depth (Figure S1a in Supporting Information S1)—extends below the northern Pamir, the Kongur Extensional System, and the northwestern Kunlun (*PL* in Figures 3a–3c and 3e). It is sandwiched between the Tarim basement *TH* and a zone of higher $V_p = 6$ –7 km/s in the central Pamir (*PH* in Figures 3a and 3e). Recovery tests indicate that *PH* and *PL* can be resolved under the given ray geometry and are not smearing artifacts from the anomalies below (Figures S10a and S10b in Supporting Information S1).

A good agreement with the receiver function Moho can be accomplished when defining the tomographic Moho at $V_p = 8$ km/s. At mantle depths (>70 km), dipping LVZs with respect to the background model are located above the seismicity in segments 1–3 (7–8 km/s, *L1*, *L2*, *L3* in Figures 3a–3c and 3f). The LVZs *L2* and *L3* of segments 2 and 3 appear continuous in map view (Figure 3f), but are separated by the seismicity of segment 2 (Figure 3b). The seismically active structures are underlain by HVZs (8.5–9.5 km/s, *H1*, *H2*, *H3* in Figures 3a–3c and 3g) and have the same dip as the LVZs above. The contrast between the LVZs and the underlying HVZs is well resolved (Figures S10a, S10b and S10d in Supporting Information S1). The location and dip of *L2* and *L3* coincide with Moho troughs identified in receiver functions (Figure S17 in Supporting Information S1; Xu et al., 2021), substantiating our observations. The HVZs are resolved to a depth of 105–120 km (Figures S10b and S10d in Supporting Information S1). *H1* and *H2* are continuous along strike below ~105 km depth (Figure 3g). *H2* and *H3* touch, but are separated by seismicity in the same way as *L2* and *L3* (Figures 3b and 3g). *L1* and *H1* as well as *L3* and *H3* dip in the same direction as the seismicity (Figures 3a and 3c).

5. Interpretation and Discussion

We visualize our interpretation of the lithospheric architecture of the central and eastern Pamir in the block diagram of Figure 4. The occurrence of earthquakes at intermediate depth requires a process that facilitates seismic failure despite high temperatures, because ductile deformation dominates below 20–30 km depth for quartz- and feldspar-, and below 50 km for olivine-dominated lithologies (Brace & Kohlstedt, 1980; Tullis & Yund, 1992). Eclogite-facies metamorphism has been found to excite intermediate-depth seismicity in oceanic subduction regimes (Incel et al., 2017; Kita et al., 2006; Yuan et al., 2000), as well as in continental lower crustal rocks (Incel et al., 2019; Jamtveit et al., 2018; John et al., 2009). Receiver function images show that upon eclogitization (in the broadest sense), the crust may become indistinguishable from the surrounding mantle in terms of seismic velocities (Rondenay et al., 2008); it may therefore yield the pattern of a LVZ shaping a local Moho trough that disappears at larger depths where the seismicity that we observe in the three segments starts. It may additionally cause densification of the slab that would promote subduction under its own weight (Ringwood & Green, 1966). The imaged velocities of *L1*, *L2* and *L3* (7–8 km/s) that are too high for non-eclogitized crust may either indicate already partial eclogitization at the onset of subduction, or result from smearing of a possibly only 10–15 km thick anomaly onto the arbitrarily but generally wider positioned inversion nodes (Sippl, Schurr, Tympel, et al., 2013); the large thickness of *L1* may result from additional pooling of more buoyant middle crust on top of the down-going plate (Sippl, Schurr, Tympel, et al., 2013). Correspondingly, Sippl, Schurr, Tympel, et al. (2013) and Mechie et al. (2019) inferred eclogitization of the lower crust of segment 1 and that this lower crust hosts the band of intermediate-depth earthquakes. In our tomogram, we interpret *L1* as the lower crust and *H1* as the mantle lithosphere of the Asian slab (Figure 3a).

The aseismic mid-crustal LVZ *PL* (Figures 3a–3c and 3e) may represent a heated rock volume, for example developed by excess radiogenic heat production in the thickened crust, viscous dissipation due to ongoing

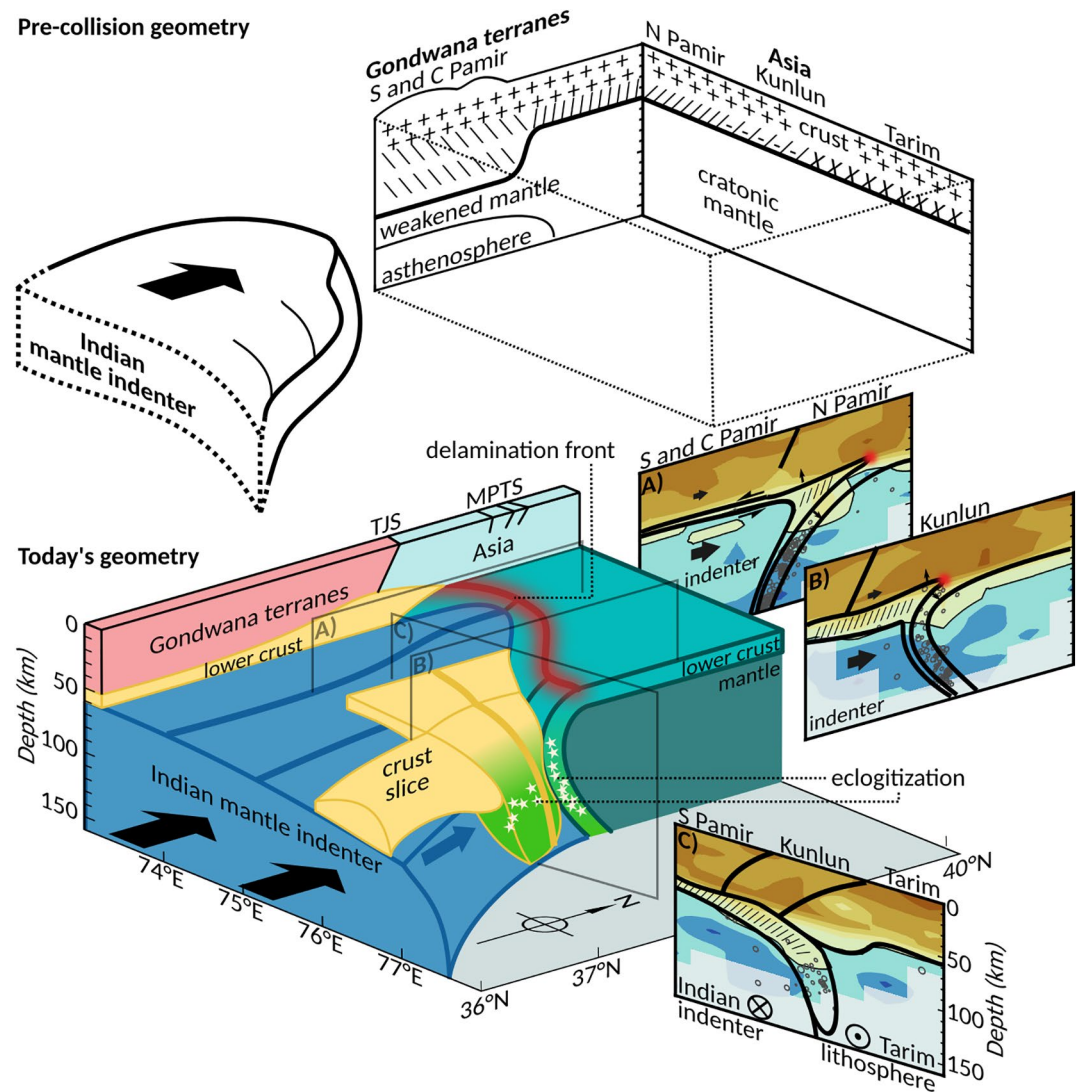


Figure 4. Structural interpretation of the V_p structure, seismicity distribution, and stresses. Top: pre-collision geometry. Bottom: interpreted block diagram of the deep lithospheric structure beneath the Pamir and northwestern Kunlun. (a–c) Interpreted cross sections of Figure 3. “///” symbols mark the lower crust involved in the collision process.

continental collision (e.g., Bird et al., 1975; Burg & Gerya, 2005) or accumulation of slab-derived fluids (Mechie et al., 2019). We can exclude anisotropy effects for PL , as seismic ray directions are well distributed (Figures S6–S9 in Supporting Information S1) and local shear-wave splitting measurements show only short delay times for the crust (Kufner, Eken, et al., 2018). Synthetic tests (Figures S10a and S10b in Supporting Information S1) and the detection of PL with surface wave tomography preclude vertical smearing from the anomalies below (W. Li et al., 2018). Most importantly, we consider heating due to asthenospheric inflow, as would be expected in the hanging wall of a S-dipping subduction zone, as unlikely, because the tomogram does not show a LVZ—characteristic of an asthenospheric wedge—south of the seismic zone; in contrast, subcrustal P -wave velocities are $>8\text{ km/s}$ with large HVZs ($>8.5\text{ km/s}$) embedded (e.g., $H3$), indicating relatively cold and rigid lithospheric mantle there.

The N-dip of the seismically active segment 2 can be traced $\sim 100\text{ km}$ along strike in narrowly adjoining profiles between 75.1 to 75.9°E (Figures S14g–S14j in Supporting Information S1) and is robust with respect to the choice of the V_p model (Figures S13g–S13j in Supporting Information S1). We interpret segment 2 as the eastern continuation of the S-dipping segment 1 of the Asian slab, because of the similar depth extent

of the seismic zone and the continuity of the underlying HVZ (Figures 2, 3a, 3b and 3g). The dip reversal suggests that the slab overturns below ~ 80 km depth (Figures 2 and 3b). Overturning in turn indicates that a force acts normal to the slab, which we expect in the presence of a pushing indenter. We attribute the seismicity gap between segments 1 and 2 to a slab tear that may explain how the slab dip changes over a relatively short distance (~ 40 km). In our interpretation, the Asian slab terminates in a seismicity cluster below the Kashgar-Yecheng Transfer System at 76.2°E (Figure 2), where, in a delamination scenario, it would need to be torn off Tarim's lithosphere to the east, where it would have originally been attached to. If instead segment 2 is separated from segment 1 and forms a continuous unit with segment 3, the Asian slab would terminate at $\sim 74.5^\circ\text{E}$ and the along-strike correlation of seismicity and $H1$ and $H2$ between segments 1 and 2 would be a coincidence.

In the northwestern Kunlun, $L3$ and $H3$ dip $\sim\text{ENE}$ and descend from the base of the Pamir crust in front of segment 2, a geometry that is also imaged by receiver functions (Figure S17 in Supporting Information S1; Xu et al., 2021). Together with the location of the seismicity band of segment 3 in front of segment 2, this geometry is inconsistent with a semicircular, amphitheater-like continuation of the Asian slab below Kunlun, but requires association of seismicity and $L3$ with another tectonic unit (see below).

The orientation of σ_1 at depth indicates that a $\text{N}13^\circ\text{W}$ compressive stress field acts on the deep structure of the Pamir. The stress orientation is stable across the three segments (Figure S16 in Supporting Information S1), although uncertainty for the individual segments may become significant, due to the varying data availability. In contrast to the observed compression, N-S extension should occur south of the slab (in segment 3), if deformation was governed by a narrow Asian slab rolling back northward (Z.-H. Li et al., 2016). We note that compressive stresses are sub-parallel to the $\text{N}12^\circ\text{W}$ ($\pm 8^\circ$)-oriented surface velocity of the southern and central Pamir crust (e.g., Ischuk et al., 2013; Metzger et al., 2020; Zubovich et al., 2010). Both are deflected about 15° counterclockwise from the $\text{N}4^\circ\text{E}$ -oriented convergence direction between India and Asia (DeMets et al., 1994). Parallelism of the orientation of the southern and central Pamir's surface displacement between the Sarez-Karakul Fault System and the Kongur Extensional System with σ_1 at depth suggests that crustal movement is prescribed by the mantle stresses, with the mantle lithosphere dragging the overlying Pamir crust south of the Asian slab northward. For segments 1 and 2, parallelism of σ_1 and surface displacement vectors arises naturally if collision occurs at an indenter tip. In summary, the repeated detection of HVZ $H3$ south of the Asian slab (this study; Mechie et al., 2012; Sippl, Schurr, Tympel, et al., 2013) that excludes asthenospheric inflow above a back-rolling subduction zone, the overturned geometry of segment 2 indicated by a change in the dip of the seismic zone, and the NNW-SSE compressive stress field across the central and eastern Pamir at mantle depth (50–100 km) that is parallel to surface displacement, support the presence of an indenter below the Pamir.

The indenter is most likely cratonic Indian lithosphere, because the Gondwana-terrane lithosphere of the central and southern Pamir and Karakorum terranes would be too weak to transmit enough force to delaminate and overturn the Asian slab (Kelly & Beaumont, 2021). We locate the delamination front at the base of the rheologically weak mid-crustal LVZ PL (red line in Figure 4), just north of the Asian slab. The present location and form of the Pamir and the Asian slab is in this interpretation governed by the shape of the indenter. Additional structural complexity, such as the location of slab tears or turn-overs, may be due to lateral changes in the strength of the indented Asian lithosphere or the along-strike variability of the indenter tip (Kelly & Beaumont, 2021; Z.-H. Li et al., 2016). For example PH , which overlies a distinctive Moho bulge in segment 1 (Figure 3a; Schneider et al., 2019), may represent a lithosphere-scale anticline; in segment 1, the top of the indenter appears to rise higher than in segment 2 and in particular in segment 3 (Figure 4).

The ENE-dipping Moho trough (Figure S17 in Supporting Information S1; Xu et al., 2021) and V_p anomalies ($L3$ and $H3$) can, in this scenario, be interpreted as Pamir crust and indenter mantle lithosphere that underthrust the Asian (Tarim) mantle lithosphere (Figure 3c). The earthquakes may, as in the Asian slab, occur in thickened crust undergoing eclogitization (Incel et al., 2019; John et al., 2009). This crust is likely dragged to depth between the bulldozing indenter and the margin of the Tarim block. The stress field of the earthquakes inside the underthrusting crust $L3$ indicates that it moves with the NNW-ward moving indenter and underthrusts the Tarim hanging wall at a highly oblique angle. As the receiver function and interpreted tomographic Moho both dip $\sim\text{WSW}$ beneath the northwestern Kunlun east of $L3$ (Figure 3c; Xu et al., 2021), we infer that Tarim underthrusts the northwestern Kunlun as well, building a stack of (from top to bottom)

Kunlun-Tarim-Pamir crust (Figure 4c). This excess crust may be responsible for a positive anomaly in the isostatic gravity residual (20-mGal-contour in Figure 2; Balmino et al., 2012) that flanks the northern edge of the Tibet plateau (Figure 2, inset), and was interpreted to represent thrusting of Tarim crust under the western and central Kunlun (Wittlinger et al., 2004).

In concert with the lack of thinned hinterland crust (Schneider et al., 2019) the herein deduced configuration of the tectonic units and the transpressive stress field in the intermediate-depth seismic zone of segment 3 preclude subduction of Asia at its (almost) entire thickness (Burtman & Molnar, 1993; Sobel et al., 2013). The detection of *H3* that is likely linked to a HVZ at ~200 km depth that has been imaged with teleseismic body and surface wave tomography and connects with the exposed Indian craton (Agius & Lebedev, 2013; C. Li et al., 2008; van Hinsbergen et al., 2019), yields a coherent picture of a promontory of Indian mantle lithosphere that underthrusts the Karakorum and the southern and central Pamir plateau between the Sarez-Karakul Fault System and the Kongur Extensional System, more than 300 km beyond the Indus suture (Figure 1). The narrow but far north reaching extent of the indenter in the Pamir suggests a strong along-strike segmentation of the northern rim of the Indian plate; it subducts under the Hindu-Kush (Kufner et al., 2021), indents in the Pamir (this study; Kufner et al., 2016) and has variable dip angles and locations beneath the rest of Tibet (e.g., Zhao et al., 2010).

6. Conclusion

The presence of an Indian mantle indenter can be inferred beneath the Pamir plateau through its high seismic velocities ($V_p > 8.5$ km/s) and the compressional stress it exerts on the overturned Asian slab. It is the farthest underthrusting part of India and the only one that refuses to subduct along the entire India-Asia plate boundary. Its plateau-defining shape needs to be accurately represented in tectonic models and gives rise to questions about the characteristics of the continental margin before collision. The likely cratonic nature of the indenter demonstrates the behavior of such lithosphere in a collision setting and can be used as a benchmark for geodynamic models.

Data Availability Statement

Seismic data was handled using *obspy* (Krischer et al., 2015) and *pyrocko* (Heimann et al., 2017). Figures were created with the help of the *Generic Mapping Tools* (Wessel et al., 2013) and *matplotlib* (Hunter, 2007), using *scientific color-maps* (Crameri et al., 2020). Seismic data are archived by GEOFON data center (<https://doi.org/10.14470/3U7560589977>, <https://doi.org/10.14470/4U7561589984>). The seismic event catalog, focal mechanism catalog and *P*-wave velocity model are available through GFZ data services (<https://doi.org/10.5880/fidgeo.2021.035>; Bloch, Schurr et al., 2021).

References

- Agius, M. R., & Lebedev, S. (2013). Tibetan and Indian lithospheres in the upper mantle beneath Tibet: Evidence from broadband surface-wave dispersion. *Geochemistry, Geophysics, Geosystems*, 14(10), 4260–4281. <https://doi.org/10.1002/ggge.20274>
- Aldersons, F. (2004). *Toward three-dimensional crustal structure of the Dead Sea region from local earthquake tomography* (PhD thesis).
- Balmino, G., Vales, N., Bonvalot, S., & Briais, A. (2012). Spherical harmonic modelling to ultra-high degree of Bouguer and isostatic anomalies. *Journal of Geodesy*, 86(7), 499–520. <https://doi.org/10.1007/s00190-011-0533-4>
- Bird, P., Toksöz, M. N., & Sleep, N. H. (1975). Thermal and mechanical models of continent-continent convergence zones. *Journal of Geophysical Research*, 80(32), 4405–4416. <https://doi.org/10.1029/jb080i032p04405>
- Bloch, W., Metzger, S., Schurr, B., Yuan, X., Ratschbacher, L., Reuter, S., et al. (2021). The 2015–2017 Pamir earthquake sequence: Fore-, main-, and aftershocks, seismotectonics and fault interaction. *Earth and Space Science Open Archive*. <https://doi.org/10.1002/essoar.10508392.1>
- Bloch, W., Schurr, B., Yuan, X., Ratschbacher, L., Reuter, S., Kufner, S.-K., et al. (2021). *Seismicity catalog, focal mechanism catalog and P-wave velocity structure between Pamir and Tarim*. GFZ Data Services. <https://doi.org/10.5880/fidgeo.2021.035>
- Brace, W., & Kohlstedt, D. (1980). Limits on lithospheric stress imposed by laboratory experiments. *Journal of Geophysical Research*, 85(B11), 6248–6252. <https://doi.org/10.1029/jb085ib11p06248>
- Burg, J.-P., & Gerya, T. (2005). The role of viscous heating in Barrovian metamorphism of collisional orogens: Thermomechanical models and application to the Lepontine Dome in the Central Alps. *Journal of Metamorphic Geology*, 23(2), 75–95. <https://doi.org/10.1111/j.1525-1314.2005.00563.x>
- Burtman, V. S., & Molnar, P. H. (1993). *Geological and geophysical evidence for deep subduction of continental crust beneath the Pamir* (Vol. 281). Geological Society of America.

Acknowledgments

We thank the drivers and field participants from the Institute of Tibetan Plateau Research, especially Hongbing Liu, who helped to organize the station deployment, Christian Sippl for sharing code and discussion and two anonymous reviewers for their helpful comments. Funded by the CaTeNA project of the German Federal Ministry of Science and Education (support codes 03G0878A and 03G0878B) and German Research Council (DFG) grant Ra 442/41. Part of the instruments were provided by GIPP of GFZ Potsdam. Open access funding enabled and organized by Projekt DEAL.

- Comino, J. Á. L., Heimann, S., Cesca, S., Milkereit, C., Dahm, T., & Zang, A. (2017). Automated full waveform detection and location algorithm of acoustic emissions from hydraulic fracturing experiment. *Procedia Engineering*, 191, 697–702. <https://doi.org/10.1016/j.proeng.2017.05.234>
- Cramer, F., Shephard, G. E., & Heron, P. J. (2020). The misuse of colour in science communication. *Nature Communications*, 11(1), 1–10. <https://doi.org/10.1038/s41467-020-19160-7>
- DeMets, C., Gordon, R. G., Argus, D. F., & Stein, S. (1994). Effect of recent revisions to the geomagnetic reversal time scale on estimates of current plate motions. *Geophysical Research Letters*, 21(20), 2191–2194. <https://doi.org/10.1029/94gl02118>
- Diehl, T., Deichmann, N., Kissling, E., & Husen, S. (2009). Automatic S-wave picker for local earthquake tomography. *Bulletin of the Seismological Society of America*, 99(3), 1906–1920. <https://doi.org/10.1785/0120080019>
- Fan, G., Ni, J. F., & Wallace, T. C. (1994). Active tectonics of the Pamirs and Karakorum. *Journal of Geophysical Research*, 99(B4), 7131–7160. <https://doi.org/10.1029/93jb02970>
- Heimann, S., Kriegerowski, M., Isken, M., Cesca, S., Daout, S., Grigoli, F., et al. (2017). *Pyrocko-An open-source seismology toolbox and library*. GFZ Data Services. <https://doi.org/10.5880/GFZ.2.1.2017.001>
- Hunter, J. D. (2007). Matplotlib: A 2D graphics environment. *Computing in Science & Engineering*, 9(3), 90–95. <https://doi.org/10.1109/MCSE.2007.55>
- Incel, S., Hilaret, N., Labrousse, L., John, T., Deldicque, D., Ferrand, T., et al. (2017). Laboratory earthquakes triggered during eclogitization of lawsonite-bearing blueschist. *Earth and Planetary Science Letters*, 459, 320–331. <https://doi.org/10.1016/j.epsl.2016.11.047>
- Incel, S., Labrousse, L., Hilaret, N., John, T., Gasc, J., Shi, F., et al. (2019). Reaction-induced embrittlement of the lower continental crust. *Geology*, 47(3), 235–238. <https://doi.org/10.1130/g45527.1>
- Ischuk, A., Bendick, R., Rybin, A., Molnar, P., Khan, S. F., Kuzikov, S., et al. (2013). Kinematics of the Pamir and Hindu Kush regions from GPS geodesy. *Journal of Geophysical Research: Solid Earth*, 118(5), 2408–2416. <https://doi.org/10.1002/jgrb.50185>
- Jamtveit, B., Ben-Zion, Y., Renard, F., & Austrheim, H. (2018). Earthquake-induced transformation of the lower crust. *Nature*, 556(7702), 487–491. <https://doi.org/10.1038/s41586-018-0045-y>
- John, T., Medvedev, S., Rüpke, L. H., Andersen, T. B., Podladchikov, Y. Y., & Austrheim, H. (2009). Generation of intermediate-depth earthquakes by self-localizing thermal runaway. *Nature Geoscience*, 2(2), 137–140. <https://doi.org/10.1038/ngeo419>
- Kelly, S., & Beaumont, C. (2021). Balanced cross-sections and numerical modeling of the lithospheric-scale evolution of the Hindu Kush and Pamir. *Journal of Geophysical Research: Solid Earth*, 126(3), e2020JB020678. <https://doi.org/10.1029/2020jb020678>
- Kita, S., Okada, T., Nakajima, J., Matsuzawa, T., & Hasegawa, A. (2006). Existence of a seismic belt in the upper plane of the double seismic zone extending in the along-arc direction at depths of 70–100 km beneath NE Japan. *Geophysical Research Letters*, 33(24). <https://doi.org/10.1029/2006gl028239>
- Krischer, L., Megies, T., Barsch, R., Beyreuther, M., Lecocq, T., Caudron, C., & Wassermann, J. (2015). ObsPy: A bridge for seismology into the scientific Python ecosystem. *Computational Science & Discovery*, 8(1), 014003. <https://doi.org/10.1088/1749-4699/8/1/014003>
- Kufner, S.-K., Eken, T., Tilmann, F., Schurr, B., Yuan, X., Mechie, J., et al. (2018). Seismic anisotropy beneath the Pamir and the Hindu Kush: Evidence for contributions from crust, mantle lithosphere, and asthenosphere. *Journal of Geophysical Research: Solid Earth*, 123(12), 10–727. <https://doi.org/10.1029/2018jb015926>
- Kufner, S.-K., Kakar, N., Bezada, M., Bloch, W., Metzger, S., Yuan, X., et al. (2021). The Hindu Kush slab break-off as revealed by deep structure and crustal deformation. *Nature Communications*, 12(1), 1–11. <https://doi.org/10.1038/s41467-021-21760-w>
- Kufner, S.-K., Schurr, B., Ratschbacher, L., Murodkulov, S., Abdulhameed, S., Ischuk, A., et al. (2018). Seismotectonics of the Tajik basin and surrounding mountain ranges. *Tectonics*, 37(8), 2404–2424. <https://doi.org/10.1029/2017tc004812>
- Kufner, S.-K., Schurr, B., Sippl, C., Yuan, X., Ratschbacher, L., Ischuk, A., et al. (2016). Deep India meets deep Asia: Lithospheric indentation, delamination and break-off under Pamir and Hindu Kush (Central Asia). *Earth and Planetary Science Letters*, 435, 171–184. <https://doi.org/10.1016/j.epsl.2015.11.046>
- Li, C., Van der Hilst, R. D., Meltzer, A. S., & Engdahl, E. R. (2008). Subduction of the Indian lithosphere beneath the Tibetan Plateau and Burma. *Earth and Planetary Science Letters*, 274(1–2), 157–168. <https://doi.org/10.1016/j.epsl.2008.07.016>
- Li, W., Chen, Y., Yuan, X., Schurr, B., Mechie, J., Oimahmadov, I., & Fu, B. (2018). Continental lithospheric subduction and intermediate-depth seismicity: Constraints from S-wave velocity structures in the Pamir and Hindu Kush. *Earth and Planetary Science Letters*, 482, 478–489. <https://doi.org/10.1016/j.epsl.2017.11.031>
- Li, Z.-H., Liu, M., & Gerya, T. (2016). Lithosphere delamination in continental collisional orogens: A systematic numerical study. *Journal of Geophysical Research: Solid Earth*, 121(7), 5186–5211. <https://doi.org/10.1002/2016jb013106>
- Liang, Y., Li, L., Liao, J., & Gao, R. (2020). Interaction of the Indian and Asian plates under the Pamir and Hindu-Kush regions: Insights from 3-D shear wave velocity and anisotropic structures. *Geochemistry, Geophysics, Geosystems*, 21(8), e2020GC009041. <https://doi.org/10.1029/2020gc009041>
- Lomax, A., Virieux, J., Volant, P., & Berge-Thierry, C. (2000). Probabilistic earthquake location in 3D and layered models. In *Advances in seismic event location* (pp. 101–134). Springer. https://doi.org/10.1007/978-94-015-9536-0_5
- Lu, S., Li, H., Zhang, C., & Niu, G. (2008). Geological and geochronological evidence for the Precambrian evolution of the Tarim Craton and surrounding continental fragments. *Precambrian Research*, 160(1–2), 94–107. <https://doi.org/10.1016/j.precamres.2007.04.025>
- Mechie, J., Schurr, B., Yuan, X., Schneider, F., Sippl, C., Minaev, V., et al. (2019). Observations of guided waves from the Pamir seismic zone provide additional evidence for the existence of subducted continental lower crust. *Tectonophysics*, 762, 1–16. <https://doi.org/10.1016/j.tecto.2019.04.007>
- Mechie, J., Yuan, X., Schurr, B., Schneider, F., Sippl, C., Ratschbacher, L., et al. (2012). Crustal and uppermost mantle velocity structure along a profile across the Pamir and southern Tien Shan as derived from project TIPAGE wide-angle seismic data. *Geophysical Journal International*, 188(2), 385–407. <https://doi.org/10.1111/j.1365-246x.2011.05278.x>
- Metzger, S., Ischuk, A., Deng, Z., Ratschbacher, L., Perry, M., Kufner, S.-K., et al. (2020). Dense GNSS profiles across the northwestern tip of the India-Asia collision zone: Triggered slip and westward flow of the Peter the First Range, Pamir, into the Tajik Depression. *Tectonics*, 39(2), e2019TC005797. <https://doi.org/10.1029/2019tc005797>
- Metzger, S., Schurr, B., Ratschbacher, L., Sudhaus, H., Kufner, S.-K., Schöne, T., et al. (2017). The 2015 Mw7.2 Sarez strike-slip earthquake in the Pamir interior: Response to the underthrusting of India's Western promontory. *Tectonics*, 36(11), 2407–2421. <https://doi.org/10.1002/2017tc004581>
- Pegler, G., & Das, S. (1998). An enhanced image of the Pamir–Hindu Kush seismic zone from relocated earthquake hypocentres. *Geophysical Journal International*, 134(2), 573–595. <https://doi.org/10.1046/j.1365-246x.1998.00582.x>
- PMP International (Tajikistan). (2005). *Tajikistan National Seismic Network*. International federation of digital seismograph networks. Retrieved from <https://www.fdsn.org/doi/10.7914/SN/TJ>

- Ringwood, A., & Green, D. (1966). An experimental investigation of the gabbro-eclogite transformation and some geophysical implications. *Tectonophysics*, 3(5), 383–427. [https://doi.org/10.1016/0040-1951\(66\)90009-6](https://doi.org/10.1016/0040-1951(66)90009-6)
- Rondenay, S., Abers, G. A., & Van Keken, P. E. (2008). Seismic imaging of subduction zone metamorphism. *Geology*, 36(4), 275–278. <https://doi.org/10.1130/g24112a.1>
- Schneider, F., Yuan, X., Schurr, B., Mechie, J., Sippl, C., Haberland, C., et al. (2013). Seismic imaging of subducting continental lower crust beneath the Pamir. *Earth and Planetary Science Letters*, 375, 101–112. <https://doi.org/10.1016/j.epsl.2013.05.015>
- Schneider, F., Yuan, X., Schurr, B., Mechie, J., Sippl, C., Kufner, S.-K., et al. (2019). The crust in the Pamir: Insights from receiver functions. *Journal of Geophysical Research: Solid Earth*, 124(8), 9313–9331. <https://doi.org/10.1029/2019jb017765>
- Schwab, M., Ratschbacher, L., Siebel, W., McWilliams, M., Minaev, V., Lutkov, V., et al. (2004). Assembly of the Pamirs: Age and origin of magmatic belts from the southern Tien Shan to the southern Pamirs and their relation to Tibet. *Tectonics*, 23(4). <https://doi.org/10.1029/2003tc001583>
- SEISDMC. (2021). *Data management centre of the China National Seismic network at the Institute of geophysics*. China Earthquake Administration. <https://doi.org/10.11998/SeisDmc/SN>
- Sippl, C., Schurr, B., Tynpel, J., Angiboust, S., Mechie, J., Yuan, X., et al. (2013). Deep burial of Asian continental crust beneath the Pamir imaged with local earthquake tomography. *Earth and Planetary Science Letters*, 384, 165–177. <https://doi.org/10.1016/j.epsl.2013.10.013>
- Sippl, C., Schurr, B., Yuan, X., Mechie, J., Schneider, F., Gadoev, M., et al. (2013). Geometry of the Pamir-Hindu Kush intermediate-depth earthquake zone from local seismic data. *Journal of Geophysical Research: Solid Earth*, 118(4), 1438–1457. <https://doi.org/10.1002/jgrb.50128>
- Sobel, E. R., Chen, J., Schoenbohm, L. M., Thiede, R., Stockli, D. F., Sudo, M., & Strecker, M. R. (2013). Oceanic-style subduction controls late Cenozoic deformation of the Northern Pamir orogen. *Earth and Planetary Science Letters*, 363, 204–218. <https://doi.org/10.1016/j.epsl.2012.12.009>
- Thurber, C. H. (1983). Earthquake locations and three-dimensional crustal structure in the Coyote Lake area, central California. *Journal of Geophysical Research*, 88(B10), 8226–8236. <https://doi.org/10.1029/jb088ib10p08226>
- Tullis, J., & Yund, R. (1992). The brittle-ductile transition in feldspar aggregates: An experimental study. In *International geophysics* (Vol. 51, pp. 89–117). Elsevier. [https://doi.org/10.1016/s0074-6142\(08\)62816-8](https://doi.org/10.1016/s0074-6142(08)62816-8)
- van Hinsbergen, D. J., Lippert, P. C., Li, S., Huang, W., Advokaat, E. L., & Spakman, W. (2019). Reconstructing Greater India: Paleogeographic, kinematic, and geodynamic perspectives. *Tectonophysics*, 760, 69–94. <https://doi.org/10.1016/j.tecto.2018.04.006>
- Waldhauser, F., & Ellsworth, W. L. (2000). A double-difference earthquake location algorithm: Method and application to the northern Hayward fault, California. *Bulletin of the Seismological Society of America*, 90(6), 1353–1368. <https://doi.org/10.1785/0120000006>
- Wessel, P., Smith, W. H., Scharroo, R., Luis, J., & Wobbe, F. (2013). Generic mapping tools: Improved version released. *Eos, Transactions American Geophysical Union*, 94(45), 409–410. <https://doi.org/10.1002/2013eo450001>
- Wittlinger, G., Vergne, J., Tapponnier, P., Farra, V., Poupinet, G., Jiang, M., et al. (2004). Teleseismic imaging of subducting lithosphere and Moho offsets beneath western Tibet. *Earth and Planetary Science Letters*, 221(1–4), 117–130. [https://doi.org/10.1016/s0012-821x\(03\)00723-4](https://doi.org/10.1016/s0012-821x(03)00723-4)
- Xu, Q., Zhao, J., Yuan, X., Liu, H., Ju, C., Schurr, B., & Bloch, W. (2021). Deep crustal contact between the Pamir and Tarim Basin deduced from receiver functions. *Geophysical Research Letters*. <https://doi.org/10.1029/2021gl093271>
- Yuan, X., Schurr, B., Bloch, W., Xu, Q., & Zhao, J. (2018). *East Pamir seismic network*. GFZ Data services. <https://doi.org/10.14470/3U7560589977>
- Yuan, X., Schurr, B., Kufner, S.-K., & Bloch, W. (2018). *Sarez Pamir aftershock seismic network*. GFZ Data services. <https://doi.org/10.14470/4U7561589984>
- Yuan, X., Sobolev, S. V., Kind, R., Oncken, O., Bock, G., Asch, G., et al. (2000). Subduction and collision processes in the Central Andes constrained by converted seismic phases. *Nature*, 408(6815), 958–961. <https://doi.org/10.1038/35050073>
- Zhao, J., Yuan, X., Liu, H., Kumar, P., Pei, S., Kind, R., et al. (2010). The boundary between the Indian and Asian tectonic plates below Tibet. *Proceedings of the National Academy of Sciences*, 107(25), 11229–11233. <https://doi.org/10.1073/pnas.1001921107>
- Zubovich, A. V., Wang, X.-q., Scherba, Y. G., Schelochkov, G. G., Reilinger, R., Reigber, C., et al. (2010). GPS velocity field for the Tien Shan and surrounding regions. *Tectonics*, 29(6). <https://doi.org/10.1029/2010tc002772>